# Encapsulation of Rh Nanoparticles Supported on $TiO_2$(110)-(1 × 1) Surface: XPS and STM Studies

**A. Berkó,* I. Ulrych,† and K. C. Prince**

*ELETTRA, Sincrotrone Trieste, S. S. 14, km 163.5 In Area Science Park, 34012 Basovizza, Trieste, Italy*

*Received: October 7, 1997; In Final Form: January 25, 1998*

The encapsulation (decoration) of Rh nanoparticles supported on a $TiO_2$(110) surface was studied by X-ray photoelectron spectroscopy (XPS) and scanning tunneling microscopy (STM). In the case of a stoichiometric and well-ordered $TiO_2$(110)-(1 × 1) surface covered by 3 monolayers (ML) of rhodium, there is no indication for thermally induced decoration of the metal particles by the suboxide phase of titania in the temperature range 300−800 K in ultrahigh vacuum (UHV). The encapsulation can be induced, however, by a few minutes annealing in a $H_2$ atmosphere of $10^{-4}$ mbar at 750 K. The islands of $TiO_x$ phase on the top of the rhodium particles were clearly detected by STM. In the case of specially grown giant Rh crystallites (diameter of 10−15 nm) annealing in $H_2$ at 750 K results in dramatic morphological changes (corrosion or disruption) of the original nanoparticles accompanying the encapsulation process. Pretreatment of the stoichiometric $TiO_2$-(110)-(1 × 1) surface by $Ar^+$ bombardment (creation of surface and subsurface $Ti^{3+}$ states) and the postdeposition of Rh on it results in encapsulation of Rh particles after annealing in UHV (in the absence of hydrogen).

## 1. Introduction

In the past few years transition metals evaporated onto the surface of oxide single crystals have been thoroughly studied by different methods mainly because they serve as a model system for oxide-supported real catalysts. To understand the elementary steps of the catalytic processes, one needs detailed information about the metal−support interaction which has a large effect on the performance of these catalysts. One of the most exciting phenomena connected to this question is the so-called strong metal−support interaction (SMSI) detected mainly on reducible oxide supports, such as titania. The most important feature characteristic for catalysts in the SMSI state is the strongly reduced capacity for CO and $H_2$ adsorption. After many years research effort it is widely accepted now that this feature can be very probably explained by *decoration (encapsulation)* of the metal nanoparticles by a suboxide phase.

The interaction between different metals evaporated onto the surface of $TiO_2$ single-crystal surfaces has been recently reviewed for example in refs 1−4. Noble metals such as Pt,[5−7] Rh,[8−11] and Pd,[12] which do not interact strongly with the support (no reduction of $TiO_2$ substrate) at room temperature, are the best known SMSI catalysts. The recent studies devoted to details of the encapsulation process on Pt-deposited $TiO_2$(110)-(1 × 1), however, show rather contradictory behavior: Pesty et al. have found strong evidence for encapsulation of the Pt nanocrystallites studied by X-ray photoelectron spectroscopy (XPS) and low-energy ion scattering (LEIS) as an effect of annealing in the temperature range 450−550 K in ultrahigh vacuum (UHV);[5,6] in contrast to this result, Schierbaum et al. using nearly the same experimental conditions and detection methods observed no evidence for encapsulation.[7] A further contradiction is found for the effect of a hydrogen ambient; Sadeghi et al. succeeded in producing the SMSI state in the case of a Rh-deposited $TiO_2$(110) surface both in UHV and in a $H_2$ background,[10,11] while it had been earlier suggested that H spillover from $H_2$ dissociation on the catalyst particles is necessary for suboxide formation and decoration to occur.[13]

Scanning tunneling microscopy (STM) studies provide mainly structural information, although the detection of current−voltage characteristics can be used for identification of the local chemical state, too. Recently we reported a detailed STM study of the thermal behavior of a Rh-deposited $TiO_2$(110)-(1 × 2) surface.[9] It was concluded that the encapsulation of Rh crystallites probably occurs as an effect of a simple thermal treatment, especially for the smallest 1−2 nm crystallites. However, it seemed to be important to apply a method that is more sensitive for the identification of the chemical state.

In this work we use XPS in order to detect the encapsulation state and to follow the effect of $Ar^+$ bombardment of the substrate before the deposition of rhodium or the result of heating of a Rh-deposited sample in $H_2$. On the basis of photoelectron spectroscopy studies, the characteristic STM images for nonencapsulated and encapsulated Rh particles are also presented. We note that in this work we use a well-ordered $TiO_2$(110)-(1 × 1) substrate for the sake of comparison with results performed with Pt-deposited titania mentioned above.[5−7] We should also mention here that in their excellent work Bernal et al. have demonstrated recently that it is possible to detect fine details of the encapsulation process on Rh/$TiO_2$ polycrystalline catalysts by high-resolution electron microscopy,[14] and it seems to be very interesting to compare these findings to those found in the case of the planar model catalyst studied in this work.

## 2. Experimental Section

The XPS measurements were carried out in a turbomolecular and ion getter pumped UHV chamber equipped with a hemi-

* Corresponding author. Permanent address: Reaction Kinetics Research Group of the Hungarian Academy of Sciences, A. József University, POB 168, H-6701 Szeged, Hungary. fax: xx- 36-62-322 378; e-mail: aberko@chem.u-szeged.hu.

† Permanent address: Institute of Physics, Czech Academy of Science, Cukrovarnicka 10, 162 00 Prague, Czech Republic.

S1089-5647(97)03255-0 CCC: $15.00 
Published on Web 04/15/1998

spherical analyzer, a double-cathode X-ray source, an electron gun for generation of AES spectra, a rearview four-grid LEED system, and an $Ar^+$ gun. The in situ treatment of the samples and the STM imaging were performed in another UHV chamber equipped with a commercial STM head (WA Technology), a three-grid AES-LEED analyzer, a quadrupole gas analyzer, an $Ar^+$ ion gun, and an auxiliary UHV-compatible transfer chamber where the treatment in $H_2$ was performed. An ultimate pressure of $5 \times 10^{-8}$ Pa was achieved in both chambers.

The polished $TiO_2(110)$ oriented samples were purchased from Crystal Tec and clipped on a Ta plate mounted on a transferable sample cartridge. Two different samples were used for XPS and STM experiments, but the well-ordered $(1 \times 1)$ structure was checked by LEED and the purity of the surface was monitored by AES measurements in both cases. Ohmic heating of a tungsten filament positioned just below a Ta plate served for annealing of the probe. The temperature of the sample in the range 300−1000 K was checked by a thin chromel−alumel thermocouple attached to the side of the sample. An infrared thermometer for independent temperature control was also used from time to time. The cleaning procedure of the $TiO_2(110)$ surface consisted of a few hours annealing at 800 K in UHV, some cycles of $Ar^+$ ion bombardement (10 min, 1 keV, $10^{-6}$ A $cm^{-2}$) at room temperature, and annealing at 900 K for 10 min in order to produce a well-ordered $1 \times 1$ reconstructed structure. This procedure resulted in some reduction of the bulk, and it increased the conductivity of the probe sufficiently for STM and photoemission measurements. In certain cases the surface stoichiometry was restored by exposing the sample at 800 K to oxygen of $10^{-6}$ mbar, but usually a few minutes annealing at 900 K was sufficient for ordering of the surface structure.

The rhodium was deposited by heating a high-purity (99.995%) Rh filament at a distance of approximately 20 mm from the sample. The amount and the purity of the epitaxial Rh overlayer were checked by Auger electron spectroscopy. The rhodium coverage was calibrated by the ratio of signal intensities ($R_{Rh}$) for Rh (302 eV) and Ti (380 eV) AES peaks, as described elsewhere (at 1 ML $R_{Rh} = 0.90$).[8,9] This calibration was supported by STM measurements performed on annealed surfaces where the Rh particles separate clearly from the support.[9] The coverage was controlled by the duration of the evaporation (deposition rate 0.2 ML $min^{-1}$).

XPS spectra were measured using Mg K$\alpha$ ($h\nu = 1253.6$ eV, glancing incidence) with detection perpendicular to the surface. STM imaging of the surface was performed by a chemically etched tungsten tip sharpened from time to time in situ by applying 5−10 V pulses or by using a continuous positive 40−70 V bias potential at 10 nA tunneling current between the tip and the sample. Tunneling conditions of +1.5 V bias and 0.2 nA tunneling current were typically used for imaging. The $256 \times 256$ points of an image were collected within 1−3 min depending on the size of the metal particles. The characteristic pictures shown in this work were chosen from many images recorded on different regions of the same sample. To avoid the imaging artifacts caused by tip convolution effects, the detection was repeated some times after heavy modification of the tip by voltage pulses.

## 3. Results and Discussion

**3.1. General Remarks.** In our previous paper a detailed STM study was presented on the deposition of Rh onto the $TiO_2$-$(110)$-$(1 \times 2)$ surface at room temperature and on the effect of annealing in UHV.[9] It was found that 3D particles with average diameter of 1−2 nm and aspect ratio of 0.3 are formed at room temperature in the low coverage range up to a few percent of a monolayer of rhodium. The average diameter of the metal particles increases to 3−4 nm at approximately monolayer coverage. Following the annealing of the $Rh/TiO_2(110)$-$(1 \times 2)$ system, the encapsulation (in the temperature range 500−700 K), the coalescence (between 700 and 900 K), and the deencapsulation of the encapsulated Rh particles (above 1000 K) were distinguished. The diameter of the largest rhodium crystallites formed by the deposition and annealing cycles described above is 5−6 nm.

In this work we study the decoration process for rhodium deposited at room temperature onto the $TiO_2(110)$-$(1 \times 1)$ surface. Although we have performed some experiments at different coverages of rhodium, we present here only the results for 3 ML coverage, because it was found by Steinrück et al. that this thickness of the epitaxial metal layer is optimal for XPS detection of the reduced $TiO_x$ phase decorating Pt nanoparticles.[5] The appearance of the decoration overlayer on the supported Rh particles and the effect of stepwise annealing in UHV were checked by XPS in two ways: (i) by detection of the change of the line shape of the Ti 2p orbital, assuming that the oxidation state of the Ti atoms is different for the encapsulated layer and for the original support; (ii) by measuring of the integrated C(1s) signal intensity of adsorbed CO detected after CO saturation at room temperature on the differently treated surfaces.

**3.2. Thermally Induced Decoration of Rhodium Deposited on Well-Ordered and $Ar^+$-Treated $TiO_2(110)$ Surfaces.** The change of the Ti 2p and Rh 3d XPS signals after deposition of rhodium at room temperature are shown for *well-ordered* (Figure 1 A,B), *slightly* (0.5 keV, $5 \times 10^{15}$ ions $cm^{-2}$) (Figure 1C,D) and *strongly* (2 keV, $5 \times 10^{16}$ ions $cm^{-2}$) (Figure 1E,F) $Ar^+$ prebombarded $TiO_2(110)$-$(1 \times 1)$ surfaces. For the two latter cases the terms "slight" and "strong" bombardment will be used in the followings. The ion sputtering was performed at an impact angle of 50° off normal. The position of the Rh $3d_{5/2}$ core level as a function of Rh coverage is plotted in Figure 2. For the well-ordered $(1 \times 1)$ surface the Rh $3d_{5/2}$ peak appeared at a binding energy of 307.6 eV and shifted to 307.0 eV. The position (458.8 eV) and the line shape of the Ti $2p_{3/2}$ level did not change, and only the intensity of this peak decreased slightly with increasing Rh coverage. Slight $Ar^+$ bombardment causes a low-energy shoulder on the Ti $2p_{3/2}$ peak, which can be explained by appearance of an XPS peak characteristic of surface $Ti^{3+}$ sites at 456.9 eV. The position of the Ti $2p_{3/2}$ peak for different oxidation states produced by ion sputtering of $TiO_2(110)$ has been presented and analyzed in detail in ref 15. This feature completely disappears already after deposition of 0.30 ML of rhodium at room temperature. The Rh $3d_{5/2}$ peak appears at 307.6 eV binding energy for the lowest coverages and shifts down to 306.9 eV. In the case of the strongly $Ar^+$ bombarded surface the Ti $2p_{3/2}$ range shows an intense shoulder at 457.0 eV, which suggests the presence of many $Ti^{3+}$ sites. This lower energy feature does not change radically as a result of 3 ML of rhodium deposited at 300 K. This behavior strongly suggests that most of these sites are localized in the subsurface region, and they are not in contact with the rhodium epitaxial layer. This suggestion is supported by the fact that the energy position of the Rh $3d_{5/2}$ peak behaves in nearly the same manner as in the two cases above: it appears at 307.4 eV and shifts to 306.8 eV. By comparison of the characteristics for the three cases in Figure 2, it can be appreciated that the shift of the binding energy starts at higher

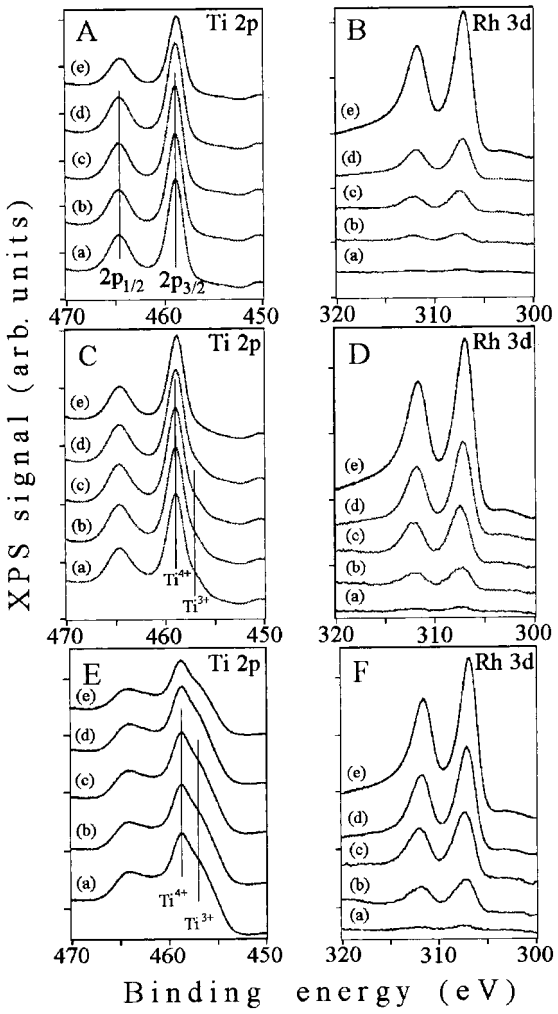


**Figure 1.** Effect of amount of Rh deposited at 300 K on the Ti 2p and Rh 3d XPS signals for well-ordered (A, B), slightly $Ar^+$-pretreated (C, D), and strongly $Ar^+$-pretreated (E, F) $TiO_2$(110)-(1 × 1) surfaces. The curves of (a), (b), (c), (d), and (e) belong to the Rh coverages of 0, 0.003, 0.030, 0.300, and 3.000 monolayer equivalents, respectively.

coverages for $Ar^+$-treated surfaces (especially for the third case). This feature may be connected to the different interaction of Rh overlayer with $Ti^{4+}$ and $Ti^{3+}$ sites in the low coverage range. The wetting ability of the epitaxial Rh is weak and results in 3D growth of the metal particles suggesting a rather weak interaction between Rh atom and the stoichiometric $TiO_2$(110) surface. The attenuation of the Ti $2p_{3/2}$ feature characteristic of surface $Ti^{3+}$ sites in Figure 1B and the differences of the shift of Rh $3d_{5/2}$ state as a function of the Rh coverage for the ordered and $Ar^+$-pretreated surfaces in Figure 2 suggest an electron transfer from $Ti^{3+}$ sites to deposited Rh atom or cluster. This observation is in good agreement with ab initio SCF calculations and photoelectron spectroscopy measurements for interaction between Pt and ideal or oxygen-defective $TiO_2$(110) surfaces.[7,16] At higher Rh coverages (>0.03 ML) the final state effects caused by the increasing size of the 3D particles strongly influence the shift in the binding energy.

The characteristic morphology detected by STM imaging for the different cases is shown in Figure 3. The overall corrugation is shown on the right bottom in the following STM images. The terrace and step structure of the clean $TiO_2$(110)-(1 × 1) surface was characterized earlier (ref 17 and refererences therein). The directions of the characteristic [001] steps are drawn in Figure 3A. After deposition of 3 ML of rhodium at 300 K on the clean $TiO_2$(110)-(1 × 1) the surface has a totally

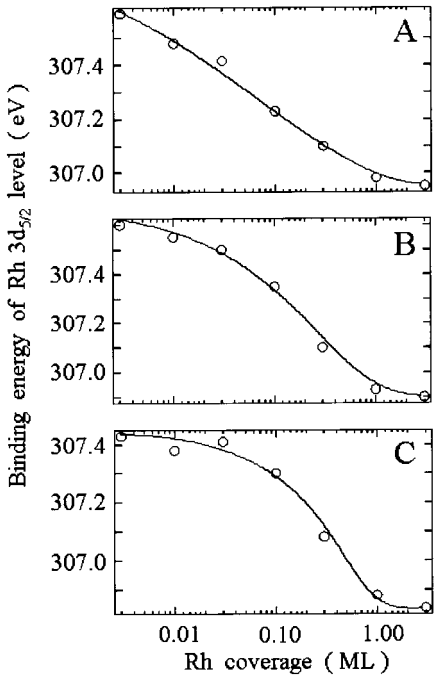


**Figure 2.** Shift of the binding energy of the Rh $3d_{5/2}$ level as a function of Rh coverage on well-ordered (A), slightly $Ar^+$-pretreated (B), and strongly $Ar^+$-pretreated (C) $TiO_2$(110)-(1 × 1) surfaces.

different morphology: the bumps with an average diameter of 3 nm can be assigned as 3D Rh particles (Figure 3B). Strong $Ar^+$ treatment also causes dramatic morphological changes: the average corrugation increases approximately 4 times; large bumps of 15 nm × 30 nm oriented in the direction of the $Ar^+$ beam are formed (Figure 3D). The detailed study of the effect of $Ar^+$ bombardment will be presented in a separate paper.[18] According to the XPS measuraments, it can be supposed that these bumps contain a large amount of $Ti^{3+}$ defect sites, and their structure is rather amorphous. The deposition of 3 ML of rhodium on this surface at 300 K causes the appearance of round features with an average diameter of 3−4 nm which can be identified as supported 3D rhodium particles (Figure 3E). It is important to remark that the average diameter of the metal particles is nearly the same for ordered and $Ar^+$-pretreated surfaces.

The effect of stepwise heating on the Ti 2p peak for ordered and $Ar^+$-treated $TiO_2$(110)-(1 × 1) surfaces were exposed to 3 ML of Rh at room temperature is shown in Figure 4. For both the ordered (Figure 4A) and slightly $Ar^+$-bombarded (Figure 4B) surfaces there is no measurable change in the shape of the Ti 2p signal; in other words, there is no sign of formation of a more reduced states in the surface region. In the case of the strongly bombarded surface (Figure 4C) the shoulder at 457.0 eV characteristic of the $Ti^{3+}$ state changes only slightly on annealing, and even after 10 min annealing at 800 K it is well detectable (see also Figure 5 B). This behavior is rather surprising because this peak totally disappears after the same annealing of the strongly $Ar^+$-treated clean $TiO_2$(110) surface (Figure 5A curves a and b). Moreover, a slight bombardment of this surface results in a decrease of the intensity of the peak characteristic of the more reduced $Ti^{3+}$ state (Figure 5 B, curve c).

The characteristic morphology of the surfaces covered with 3ML of rhodium and annealed in UHV at 800 K can be seen in Figure 3C,F. For both the ordered and the strongly $Ar^+$ ion pretreated surfaces the average diameter of the rhodium nanocrystallites increases from 3 to 4 nm (measured before annealing)

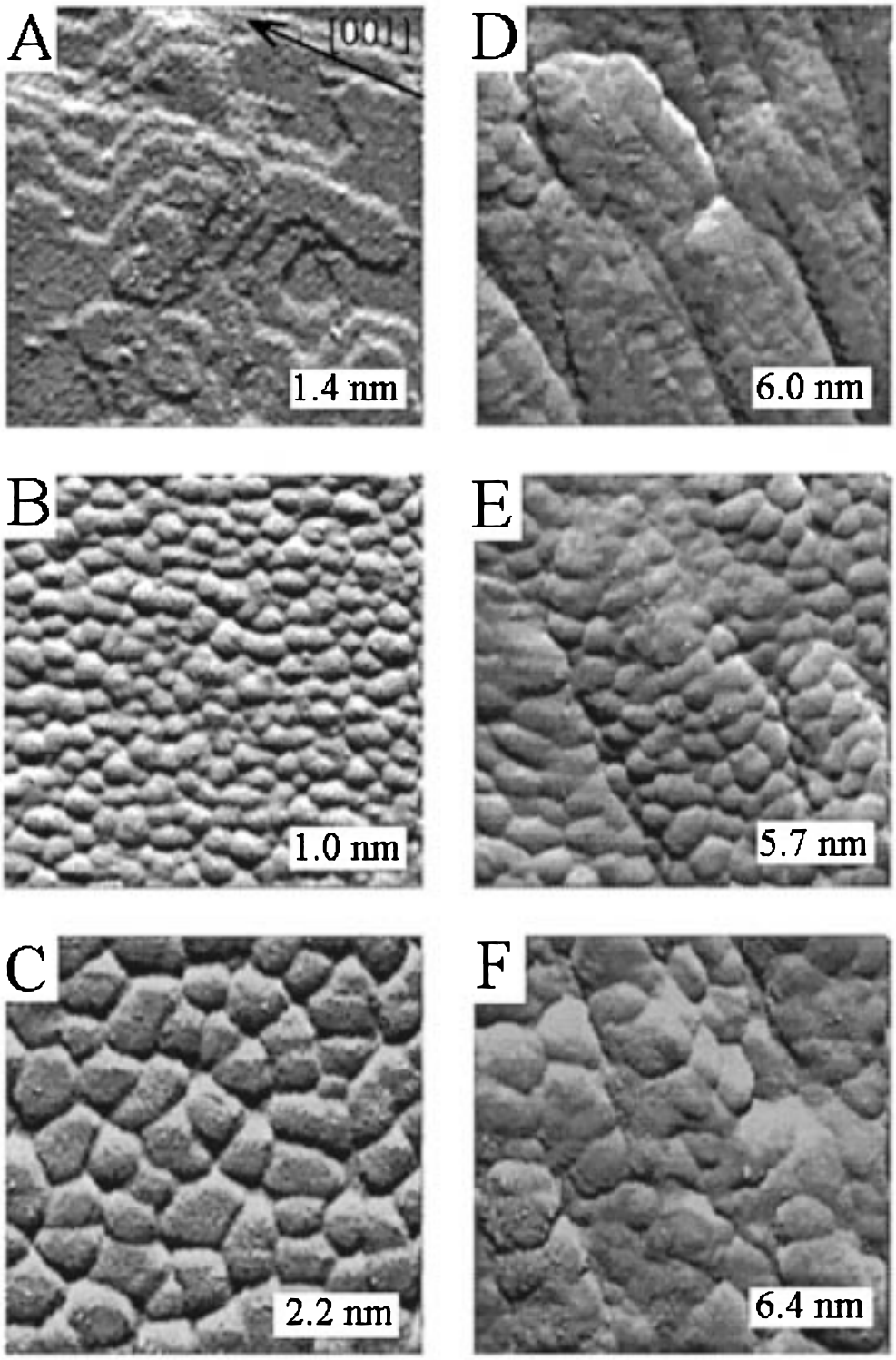


**Figure 3.** Characteristic STM images for well-ordered (A, B, C) and strongly $Ar^+$-pretreated (D, E, F) $TiO_2(110)$-$(1 \times 1)$ surfaces before deposition of Rh (A, D), after deposition of 3 ML of Rh at 300 K (B, E), and following annealing at 800 K in UHV (C, F). Size of the images: 50 nm × 50 nm.

up to 5−6 nm. In the case of the latter surface the large overall corrugation caused by the ion bombardment pretreatment does not change remarkably; in other words, there is no intensive mass transport from the subsurface region of the titania support. Because of the large corrugation of this surface, it is difficult to resolve the top structure of the Rh particles. In the case of the ordered $TiO_2(110)$-$(1 \times 1)$ surface the top plane of the particles seems to be rather flat.

In the case of the ordered and strongly $Ar^+$-bombarded surfaces covered by 3 ML of rhodium at room temperature, the CO exposure (saturation) results in the appearance of an intense XPS signal at 285.8 eV, which is characteristic of adsorbed CO bonded to Rh particles (Figure 6 A,C). The annealing of the ordered surface covered by 3 ML of rhodium at 800 K in UHV causes only a slight decrease of the amount of CO saturation for the clean $TiO_2(110)$ surface (Figure 5B). The CO uptake is however strongly diminished after the same thermal treatment for the strongly $Ar^+$-bombarded surface (Figure 5D). Table 1 contains the relative amount of CO adsorbed in saturation for the three different surfaces discussed in this section. The values

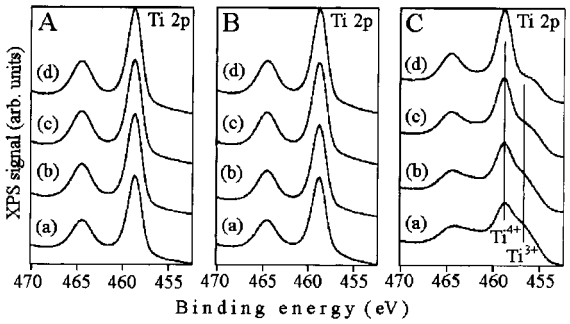


**Figure 4.** Change of Ti 2p XPS signal after annealing of differently pretreated $TiO_2$(110)-(1 × 1) surfaces covered by 3 ML of Rh at 300 K (a) and after annealing at 550 K (b), 700 K (c), and 800 K (d) for 10 min in UHV. Stoichiometric (A), slightly (B), and strongly (C) $Ar^+$-pretreated surface.

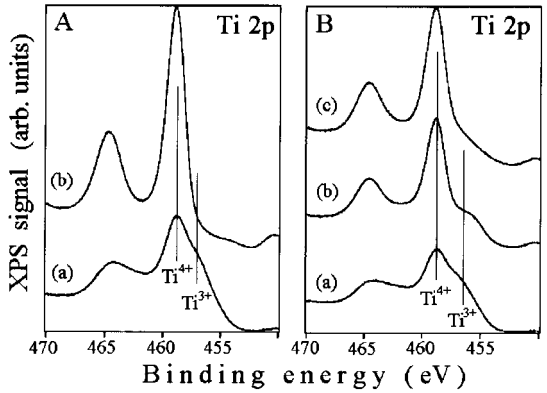


**Figure 5.** Effect of annealing in UHV on the Ti 2p XPS signal of strongly $Ar^+$-treated $TiO_2$(110)-(1 × 1) (A) and of the same surface exposed to 3 ML of rhodium at room temperature (B). Before annealing (a); after 10 min at 800 K in UHV (b); after a slight $Ar^+$ treatment of the Rh-covered and annealed sample (c).

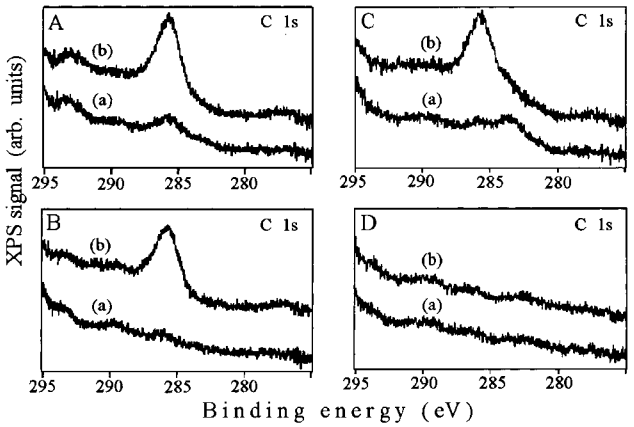


**Figure 6.** C 1s XPS signals recorded before and after exposure to CO (6 langmuirs) at 300 K on different Rh/$TiO_2$ surfaces, (a) and (b) curves, respectively. $TiO_2$(110)−(1 × 1) surface covered by 3 ML of Rh at 300 K (A); the same surface after 10 min annealing at 800 K (B); strongly $Ar^+$-treated and covered to 3 ML of Rh at 300 K (C); the same surface after 10 min annealing at 800 K (D).

collected in this table were calculated from the integrated area of C 1s signal (after normalizing to the Ti 2p peak) of adsorbed CO. The amount of CO adsorbed before annealing does not show strong variation (lower than 10−15%) for the different cases. In contrast to this behavior annealing at 800 K causes a completely different situation. In the cases of ordered and slightly $Ar^+$-treated surfaces, the CO saturation decreases by approximately 30−40% which can be explained by annealing-induced agglomerization of the epitaxial Rh. At the same time

**TABLE 1: Effect of $Ar^+$ Pretreatment and Subsequent Annealing on the Capacity for CO Uptake at 300 K (Relative Integral Intensity of the Characteristic C(1s) Peak)**

| | 3 ML of Rh at 300 K | after 10 min annealing in UHV at 800 K |
|---|---|---|
| (1 × 1) ordered | 97 | 66 |
| slightly $Ar^+$-sputtered | 100 | 58 |
| strongly $Ar^+$-sputtered | 83 | <2 |

there is a very intensive attenuation (more than 98%) in the capacity for CO uptake on the strongly $Ar^+$-bombarded surface. This latter phenomenon cannot be explained simply by agglomeration of the Rh particles as the STM measurements show (see above).

From the experimental results presented above some conclusions can be drawn about the thermal activation of the encapsulation process of Rh crystallites supported on $TiO_2$(110)-(1 × 1) surface. As the reduction of the CO uptake is moderate on the ordered and the slightly $Ar^+$-treated surfaces, it means that no encapsulation of the Rh particles occurs in these cases. This is supported by STM measurements performed on the ordered titania surface, where the top plane of the Rh crystallites are rather flat after annealing in UHV at 800 K (Figure 3C). This conclusion is valid for the titania support containing mainly surface oxygen defects (after slight $Ar^+$ bombardment). In contrast to these cases clear evidence was found for encapsulation of the Rh crystallites in the case of the strongly $Ar^+$ presputtered surface: (i) substantial attenuation of ability for CO adsorption; (ii) the XPS detection of the Ti 2p state characteristic of $Ti^{3+}$ sites even after annealing at 800 K in UHV, moreover the disappearance of this feature after gentle $Ar^+$ bombardment. Unfortunately, the high corrugation of this latter surface prevented the clear imaging of the decoration layer by STM.

**3.3. Effect of Annealing of Rh-Deposited $TiO_2$(110)−(1 × 1) Surface in $H_2$.** It was demonstrated above that in the case of a well-ordered $TiO_2$(110)-(1 × 1) surface the epitaxial Rh is not encapsulated by annealing in UHV. In this section the effect of a $H_2$ ambient is studied for this type of surface. The appearance of the decoration overlayer after annealing in a hydrogen atmosphere was checked by measuring the C 1s signal of adsorbed CO detected after CO saturation. Figure 7A shows the relative amount of CO at saturation (calculated from the integral of C 1s XPS signal of adsorbed CO) for the samples covered by 2.5 ML of Rh at room temperature and treated in increasing $H_2$ pressure at 750 K for 10 min. The lowest pressure at which well-measurable attenuation in the CO uptake appears is $10^{-4}$ mbar (Figure 7A, a−d). This surface can be easily reactivated by slight $Ar^+$ bombardment (Figure 7A, e). The formation of the SMSI state as a function of duration was followed in $10^{-4}$ mbar of $H_2$ pessure and is plotted in Figure 7B. The change of Ti 2p signal as a function of duration of annealing in $10^{-4}$ mbar of $H_2$ can be seen in Figure 7C. Although there is no appreciable change in the shape of the Ti $2p_{3/2}$ spectra, the very low amount of CO uptake clearly shows the presence of a decorating overlayer (Figure 7B). As the CO uptake is decisive evidence for encapsulation, we suppose that the stoichiometry of titania overlayer is close to that of $TiO_2$. It is probable that the oxygen diffusion from the subsurface is sufficiently fast for reoxidation of the titania overlayer after closing the $H_2$ flow. In the case of the $Ar^+$-treated surface this latter process is less probable because of the oxygen-deficient subsurface.

The STM images recorded before and after the treatment in $H_2$ show well-distinguishable differences in the morphology of

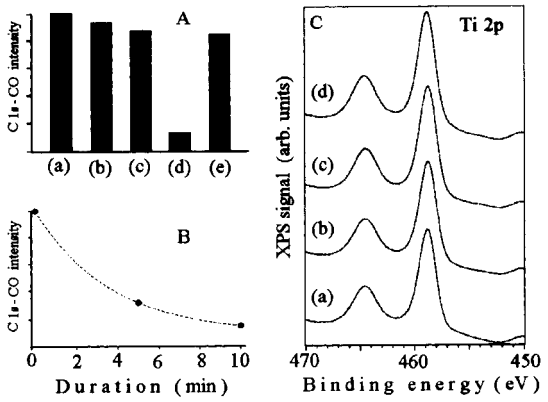


**Figure 7.** Effect of different treatments on CO uptake on $TiO_2$(110)-(1 × 1) surface deposited by 2.5 ML of Rh (A): 10 min annealing at 750 K in UHV (a), in $H_2$ pressure of $10^{-6}$ mbar (b), $10^{-5}$ mbar (c), $10^{-4}$ mbar (d), and a gentle $Ar^+$ treatment at room temperature (e). The amount of adsorbed CO was calculated by relative integrated area of the C 1s peak. Effect of duration on CO uptake for annealing at 750 K in $10^{-4}$ mbar of $H_2$ (B). Change of Ti 2p XPS signal detected on the same surface after the different treatments (C): annealing in UHV at 750 K for 10 min (a); 2 and 10 min treatment at 750 K in $10^{-4}$ mbar of $H_2$, (b) and (c), respectively; after a gentle $Ar^+$ treatment (d).

the particles (Figure 8 A,B). In the case of annealing at 800 K in UHV the edges of the particles are rather sharp, and the top plane is quite flat. The annealing in $H_2$ induces the appearance of structures which jut out from the top of the particles. This is clearly seen also on the line profiles (Figure 8C,D). Although from the STM images it is rather difficult to identify the material of these extra features, nevertheless on the basis of the XPS measurements these features can be assigned as $TiO_x$ decoration of the Rh particles, where $x$ is close to 2. These forms possibly represent a discontinuous rather than a complete covering layer. (Otherwise, it would be rather difficult to detect by STM.) This islandlike structure of the decoration layer was observed recently in the case of polycrystalline $Rh/TiO_2$ catalysts by high-resolution electron microscopy.[14] From the fact that partly covered surfaces do not adsorb CO, it can be concluded that an electronic effect also plays some role in the inhibition of CO adsorption. This is in good agreement with the conclusions obtained on Pt and Rh foils and single crystals covered partly by an evaporated $TiO_x$ overlayer.[19−24]

A special preparation method was applied to produce well-separated giant Rh crystallites (diameter above 10 nm), which is described in detail elsewhere.[25] The method consists of evaporation of a small quantity of Rh (less than 1% of one monolayer) at room temperature with subsequent annealing at 1100 K in UHV. This seeded surface, where the average distance between the particles depended sensitively on the Rh coverage (in the range 0.1−10% of a monolayer), was exposed to further rhodium at 1100 K. This latter deposition resulted in the growth of the existing small crystallites (seeds) depending on the amount of rhodium evaporated in the second part of the preparation. To follow the change of morphology due to encapsulation induced by $H_2$, a surface characterized by the STM image (200 nm × 200 nm) in Figure 8E was used. Basically two different types of Rh crystallites can be found: hexagonal coin-shaped nanoparticles and strongly elongated crystallites oriented in the [001] direction of the support. This surface texture radically changes after 10 min annealing at 750 K in $10^{-3}$ mbar of $H_2$: a general tendency is that the larger particles disrupt into smaller ones (Figure 8F,G). The fact that the structural changes appear at nearly the same $H_2$ pressure and temperature as for the cases above suggests that the metal particles are in an encapsulated state, although this type of surface was not checked in situ by XPS.

**3.4. Mechanism of Encapsulation of Noble Metals Supported by Titania.** The encapsulation of Rh, Pt, Pd, and Ru particles by support oxides has been verified in detail by different spectroscopic methods, but there are only a few works devoted to the structural characterization of this process.[14,26,27] They are rather contradictory, surprisingly even in the case of structurally and chemically well-characterized planar catalysts.[5−7] In this section we concentrate on two important questions of the encapsulation process: (i) what is the role of the $Ar^+$ pretreatment on formation of the encapsulating oxide layer, and (ii) does the encapsulation cause any structural modification of the supported metal particles?

As we have demonstrated above, the low-intensity and -energy $Ar^+$ sputtering of the well-ordered $TiO_2$(110) results in mainly surface oxygen defects and alters the interaction between the Rh atoms or clusters and the oxide substrate. Nevertheless, this pretreatment does not induce the encapsulation of the metal particles on annealing in UHV. However, the more intensive sputtering at higher energy results in reduction of the subsurface region of the support material and in the encapsulation of the Rh particles after postannealing in UHV. This behavior clearly suggests that the encapsulation depends mainly on the diffusion of the reduced $TiO_x$ species. In the classical method for inducing the encapsulated state, i.e., annealing at high temperature in a $H_2$ atmosphere, the first step is the formation of a reduced phase.[14] Our results exclude the possibility that the encapsulation can start on a well-ordered $TiO_2$(110)-(1 × 1) surface, although the process starts readily in a $H_2$ atmosphere. This observation resolves the earlier contradiction found by Sadeghi and Henrich; i.e., the encapsulation of Rh crystallites supported on $TiO_2$(110) proceeded surprisingly indepedent of $H_2$ pressure.[10,11] Two explanations can be given: (i) hydrogen dissolved in the bulk induced the formation of the decoration overlayer after annealing; (ii) the long-term handling (annealing, treatments in hydrogen, $Ar^+$ sputtering) of the sample caused a drastic decrease in bulk oxygen able to diffuse to the surface. These properties may also give an explanation for the different behavior for $Pt/TiO_2$-(110) system found in refs 3 and 4 and call attention to the need for a better characterization of the subsurface state for these experiments. The oxidation state of the encapsulation titania layer may be very close to $Ti^{4+}$, as no reduced state was found in this work after the treatment in $H_2$. This observation shows that the Ti 2p signal alone does not give certain information about the existence of a decoration overlayer. It is worth mentioning here that the thermally induced (1 × 1) → (1 × 2) phase transition detected on a clean $TiO_2$(110) surface is also sensitive to subsurface conditions, as was concluded recently.[17,28] This fact may explain why the supported Rh nanoparticles encapsulate on $TiO_2$(110)-(1 × 2) surface on annealing in UHV.[9]

In a very recent paper Gao et al. came to nearly the same conclusion about the role of the subsurface stoichiometry of a $TiO_2$ support in a study of Pt/Nb-doped $TiO_2$(100) system.[29] It was found that considerable suppression of the decoration process for Pt supported on $TiO_2$(100) can be achieved by reducing oxygen vacancy defect densities in the bulk and by doping the near-surface region with Nb.

In some earlier work it was shown that the encapsulation process is accompanied by structural changes of the metal particles themselves, namely, the metal particles spread over the support.[30−32] The later studies however did not provide any

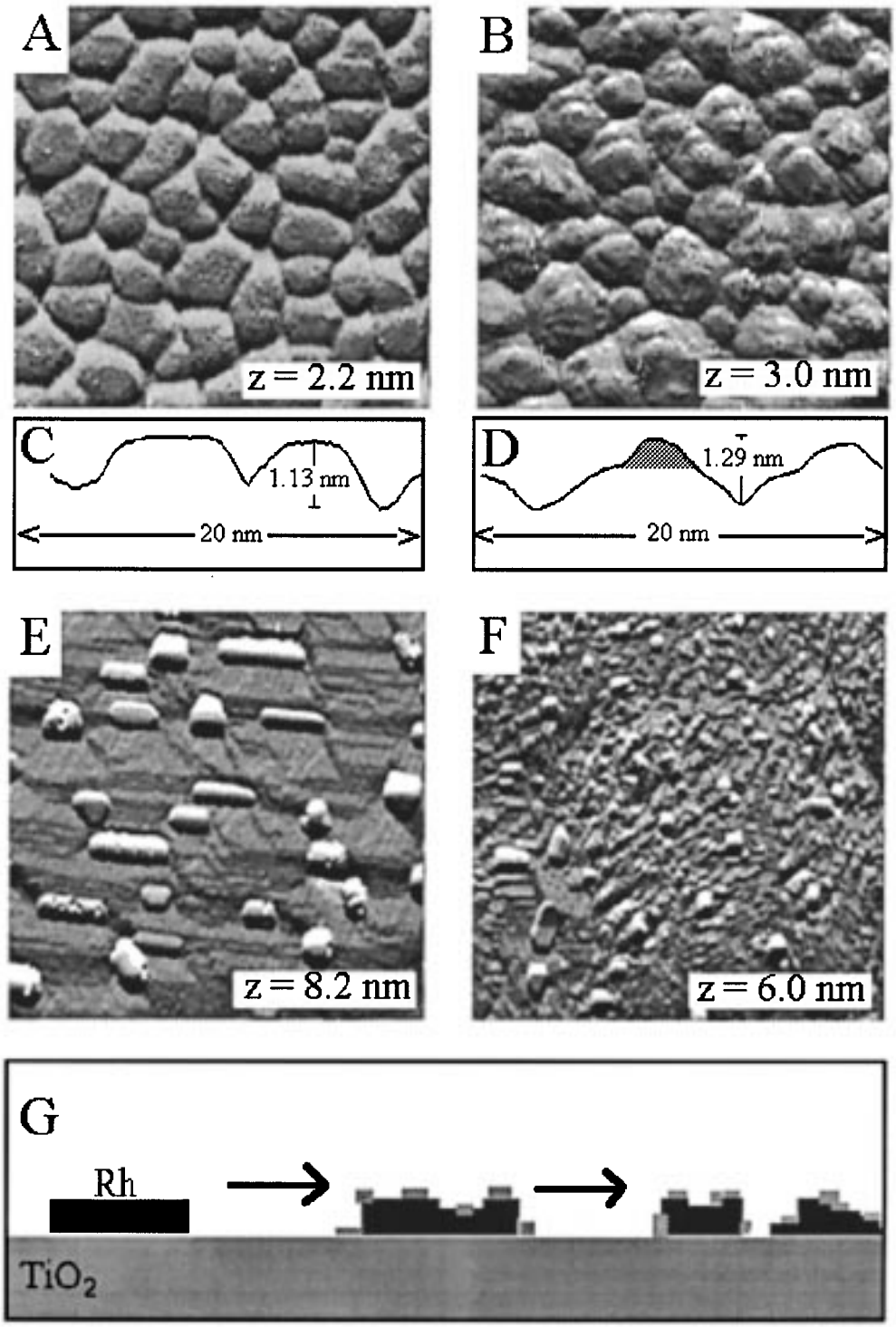


**Figure 8.** Typical STM images (50 nm × 50 nm) for a $TiO_2$(110)-(1 × 1) surface covered by 3 ML of Rh and annealed in UHV at 800 K (A). The same surface after annealing at 750 K in $10^{-3}$ mbar of $H_2$ for 10 min (B). The 20 nm line profiles (C) and (D) recorded for (A) and (B), respectively. STM images (200 nm × 200 nm) of specially grown giant Rh crystallites (see text) supported on the $TiO_2$(110) surface before and after thermal treatment at 750 K in $10^{-3}$ mbar of $H_2$ (E, F). The suggested mechanism for the encapsulation (G).

evidence for dramatic morphological changes apart from some sintering of the metal particles.[15,33] In this work very intensive disruption of the supported Rh nanoparticles was clearly demonstrated by STM for the giant metal crystallites (>10 nm). This observation prompted a study of the fine details of this process which will be published in the near future. The driving force for this process may be the lower total surface energy as a result of increased contact region between the noble metal and the encapsulation oxide. Regarding the size of the metal particles and the stoichiometry of the decoration phase, it seems to be very likely that there is an optimal particle diameter for minimization the total surface energy.

## 4. Conclusions

The 3D Rh nanoparticles formed by evaporation of Rh at room temperature onto the well-ordered $TiO_2$(110)-(1 × 1) surface are not encapsulated after annealing up to 900 K in UHV. In contrast to this behavior, the decoration of the supported Rh particles can be induced readily on strongly presputtered and postdeposited $TiO_2$(110)-(1 × 1) surfaces by

a few minutes annealing at 750 K in UHV. Moreover, the presence of $10^{-4}$ mbar of $H_2$ during annealing results in the formation of a decoration layer of $TiO_x$ phase even in the case of the well-ordered of $TiO_2(110)$-$(1 \times 1)$ surface covered by rhodium. On the top of the coin-shaped Rh particles the decoration islands were clearly observed by STM imaging. The specially grown giant Rh crystallites (average diameter of more than 10 nm) decompose into smaller particles during the encapsulation process induced by thermal treatment in $H_2$ ambient.

**Acknowledgment.** This work was supported by Copernicus Program of the European Community, CIPA-CT94-0217. The authors express their thanks to Prof. F. Solymosi (Reaction Kinetics Research Group of the Hungarian Academy of Sciences) for allowing to perform some STM measurements and to Dr A. Baraldi and Mr L. Romanzin (ELETTRA, Sincrotrone Trieste) for helpful discussions and assistance.

## References and Notes

(1) Diebold, U.; Pan, J. M.; Madey, T. E. *Surf. Sci.* **1995**, *331*−*333*, 845.
(2) Cambell, C. T. *Surf. Sci. Rep.* **1997**, 27, (1−3), 1.
(3) Goodman, D. W. *Surf. Rev. Lett.* **1996**, *2*, 9.
(4) Lad, R. J. *Surf. Rev. Lett.* **1995**, *2*, 109.
(5) Pesty, F.; Steinrück, H.-P.; Madey, T. E. *Surf. Sci.* **1995**, *339*, 83.
(6) Steinrück, H. P.; Pesty, F.; Zhang L.; Madey, T. E. *Phys. Rev. B* **1995**, *51*, 2427.
(7) Schierbaum, K. D.; Fischer, S.; Torquemada, M. C.; Segovia, J. L.; Román E.; Martin-Gago, J. A. *Surf. Sci.* **1996**, *345*, 261. Fisher, S.; Schneider, F.; Schierbaum, K. D. *Vacuum* **1996**, *47* (10), 1149.
(8) Poirier, G. E.; Hance, B. K.; White, J. M. *J. Phys. Chem.* **1993**, *97*, 5965.
(9) Berkó, A.; Ménesi, G.; Solymosi, F. *Surf. Sci.* **1997**, *372*, 202.
(10) Sadeghi, H. R.; Henrich, V. E. *Appl. Surf. Sci.* **1984**, *19*, 330.
(11) Sadeghi, H. R.; Henrich, V. E. *J. Catal.* **1984**, *87*, 279.
(12) Zhang, L.; Diebold U.; Madey, T. E. Manuscript in preparation.
(13) Resasco, D. E.; Haller, G. L. *J. Catal.* **1983**, *17*, 279.
(14) Bernal, S.; Botana, F. J.; Calvino, J. J.; López, C.; Pérez-Omil J. A.; Rodriguez-Izquierdo, J. M. *J. Chem. Soc., Faraday Trans.* **1996**, *92* (15), 2799.
(15) Mayer, J. T.; Diebold, U.; Madey, T. E.; Garfunkel. E. *J. Electron Spectrosc. & Relat. Phenom.* **1995**, *73*, 1.
(16) Wei-Xing, X.; Schierbaum, K. D.; Goepel, W. *J. Solid State Chem.* **1995**, *119*, 237.
(17) Berkó, A.; Solymosi, F. *Langmuir* **1996**, *12*, 1257.
(18) Berkó, A.; Solymosi, F. Unpublished results.
(19) Levin, M. E.; Salmeron, M.; Bell, A. T.; Somorjai, G. A. *Surf. Sci.* **1986**, *169*, 123.
(20) Levin, M. E.; Williams, K. J.; Salmeron, M.; Bell, A. T.; Somorjai, G. A. *Surf. Sci.* **1988**, *195*, 341.
(21) Wang, H. C.; Ogletree, D. F.; Salmeron, M. *J. Vac. Sci. Technol. B.* **1991**, *9* (2), 853.
(22) Boffa, A. B.; Galloway, H. C.; Jacobs, P. W.; Betínez, J. J.; Batteas, J. D.; Salmeron, M.; Somorjai, G. A. *Surf. Sci.* **1995**, *326*, 80.
(23) Ko, C. S.; Gorte, R. J. *J. Catal.* **1984**, *890*, 59.
(24) Ko, C. S.; Gorte, R. J. *Surf. Sci.* **1985**, *161*, 597.
(25) Berkó A.; Solymosi, F. *Surf. Sci.*, in press.
(26) Braunschweig, E. J.; Logan, A. D.; Datye, A. K.; Smith, D. J. *J. Catal.* **1989**, *118*, 227.
(27) Dartye, A. K.; Kalakkad, D. S.; Yao, M. H.; Smith, D. J. *J. Catal.* **1995**, *155*, 148.
(28) Baker, R. T. K.; Prestidge, E. B.; Garten, R. L. *J. Catal.* **1979**, *56*, 390.
(29) Gao, Y.,; Liang, Y.; Chambers, S. A. *Surf. Sci.* **1996**, *365*, 638.
(30) Guo, Q.; Cocks, I.; Williams, E. M. *Phys. Rev. Lett.* **1996**, *77* (18), 3851.
(31) Baker, R. T. K.; Prestidge, E. B.; Garten, R. L. *J. Catal.* **1979**, *59*, 293.
(32) Singh, A. K.; Pande N. K.; Bell, A. T. *J. Catal.* **1985**, *94*, 422.
(33) Tauster, S. J. *Acc. Chem. Res.* **1987**, *20*, 389.